Viscoelastic Model for Particle Fragmentation in Olefin Polymerisation

ARTICLE *in* AICHE JOURNAL · JUNE 2003

Impact Factor: 2.75 · DOI: 10.1002/aic.690490613

3 AUTHORS, INCLUDING:

Hallvard F. Svendsen
Norwegian University of Science and Techno…
267 PUBLICATIONS **4,963** CITATIONS
SEE PROFILE

Timothy F.L. McKenna
Centre National de Recherche Scientifique, L…
215 PUBLICATIONS **2,548** CITATIONS
SEE PROFILE

Viscoelastic Model for Particle Fragmentation in Olefin Polymerization

Pål Kittilsen and Hallvard F. Svendsen
Dept. of Chemical Engineering, Norwegian University of Science and Technology (NTNU), N-7491 Trondheim, Norway

Timothy F. McKenna
LCPP-CNRS/ESCPE-Lyon, Bât F308, 43 Blvd du 11 Novembre 1918, 69616 Villeurbanne Cedex, France

The catalyst particle fragmentation process is an important step in determining the final morphology of olefin polymer particles. Understanding the different phenomena that influence it is, therefore, essential in optimizing polymerization processes and in obtaining the desired quality of polymer. A new viscoelastic model of the fragmentation process developed is demonstrated. The model relates the magnitude and generation rate of physical forces and the physical characteristics of the polymer and support. In this way, the effects of different parameters, such as reaction rate, polymer properties, and support characteristics, can be related to changes in the morphology of polymer particles. A faster reaction rate makes the particle become more porous, and a more viscous polymer will make particles with less porosity. It is discussed why larger pores will break before smaller on the same catalyst.

Introduction

At an annual production of 85–95 million tons, polyolefins are by far the plastic materials with the highest levels production worldwide (for example, McKenna and Soares, 2001). The most common way of producing polyolefins is using heterogeneous catalysis. These catalysts are typically porous particles on the order of 10–100 μm in diameter, which are injected into a reactor containing olefin monomers in either a gaseous or liquid state. The active sites upon which the polymer is formed are deposited on the internal surfaces of the pores in the particle. Formation of polymer inside the pores eventually causes the catalyst particles to fragment, and then expand into particles with diameters approximately 10 to 50 times larger than the original catalyst particles. The fragments of the catalyst remain in the polymer.

It is a well accepted fact that the particle fragmentation process is an extremely important step in determining the final morphology of a growing catalyst/polymer particle, and that it can have a strong influence on the observed kinetics during the polymerization reaction (for example, Laurence and Chiovetta, 1983; Galli, 1999; Galli and Haylock, 1991; Webb et al., 1991; Pater et al., 1998; Weickert et al., 1999). In addition, morphological characteristics of the polyolefin powder, including the particle-size distribution (PSD), porosity (ϵ), and bulk density (ρ_{bulk}) are important quality parameters. These characteristics will be determined in large part by the morphology at the end of the fragmentation step. There is a clear need for a model relating the magnitude and rate of generation of the physical forces present and the physical characteristics of the particle itself (that is, physical resistance of the catalyst support and viscoelastic properties of the polymer matrix). As has been discussed recently in the literature, it is not possible to develop quantitative descriptions of particle growth without a representation of the particle morphology (Kittilsen et al., 2001; McKenna and Soares, 2001).

The structure of the catalyst particles varies with the type of support material. The two most common materials are $MgCl_2$ and SiO_2. $MgCl_2$ particles are made of a complex agglomeration of small crystallites, whereas the silica particles have a branched pore network in a continuous gel (Ferrero and Chiovetta, 1992a). This difference, coupled with the different chemistries found on the two types of support,

Correspondence concerning this article should be addressed to T. F. McKenna.
Current address of P. Kittilsen: Norsk Hydro, Corporate Research Center, Porsgrunn, Norway.

means that the fragmentation process also will be different. It is believed that $MgCl_2$-supported particles fragment quite uniformly by the breakage of the relatively weak bonds between the crystallites, forming an agglomeration of small polymer particles with catalyst fragments inside. This representation of particle morphology led to the development of the well-known multigrain model [MGM; see, for example, Floyd et al. (1986a)]. One common assumption when using the MGM is an instant and complete fragmentation of the catalyst. This assumption has been found to be a good approximation for many $MgCl_2$-supported Ziegler–Natta catalysts because they fragment rapidly and are composed of small crystallites, but not for the SiO_2-supported catalyst, because the fragmentation process can take much longer and the structure of the particles is not conducive to the same pattern of rupturing (for example, Ferrero et al., 1992, 1993). SiO_2-supported particles seem to fragment in a more progressive way, starting by fragmentation at the larger pores, and continuing successively with the smaller pores. The support is ground into smaller fragments.

Despite the importance of this subject, very little work has been done on trying to model the relationship between the reaction rate, properties of the polymer, and particle fragmentation. Laurence and Chiovetta (1983) were the first to treat this subject in detail. They imposed a model of morphology based on the MGM, and allowed the particle to fragment on a layer-by-layer basis. It was assumed that the particle fragmented when a certain (arbitrary) amount of polymer was deposited on the active sites at a given position, and that the rates of diffusion were different in the fragmented and unfragmented parts of the particle. While interesting, this and later extensions of this concept (Ferrero and Chiovetta, 1987a,b, 1991a,b) remained very simple, and did not allow polymer properties or the rate of reaction to be directly related to particle morphology. A more fundamental study was presented by Estenoz and Chiovetta (1996), who proposed a model in which the actual porosimetry data of the catalyst and the polymer particles were used. Changes in the morphology during the initial fragmentation step were studied in terms of the total particle surface area and pore volume. Although the model was adapted to data from silica supports, it was generic enough that it should be possible to predict the development of the fragmentation process of other systems with porosimetry data from any system. However, as mentioned earlier, the limitation of this work is that the fragmentation step is not directly related to polymer properties, the rate of reaction, or to the reaction conditions.

Kosek et al. (2001a,b) proposed another interesting approach based on a full-scale representation of the morphology of a particle. The starting point is a 3-D model of the catalyst particle obtained from SEM, TEM, or X-ray tomography data of real particles. The morphology (shape, pore distribution) of polymer particles is simulated in 3-D by a Monte-Carlo-like simulation. A kinetic model is used to describe the rate of polymer formation on the pore walls of the support material, and the breakage and further expansion of the particle are simulated, giving the final morphology of the particle. This approach seems to be very promising, and future developments in this direction will most likely be forthcoming from this group.

As polymer is deposited on the catalyst surface, it starts to create a resistance to the deposition of more polymer. This resistance, or stress, is what eventually causes the support to rupture. The driving force of this process is the osmotic pressure caused by the dissolved monomer molecules in the polymer matrix. A detailed study of these effects was done by Agarwal (1998) and Agarwal and Lemstra (2001). First they estimated the viscous, and then the viscoelastic effects of the deposited polymer on the rate of reaction. The work essentially concerned the deformation of the polymer layer around the active sites, and how this deformation influenced monomer transfer through the polymer layer toward the active sites. To the best of our knowledge, Agarwal (1998) was the first to try to model viscous deformation at the level of the micrograins in a growing polymer particle. However, neither of these two articles considers the process of particle rupture and the influence of the reaction rate on stress generation, and, thus, on the generation of forces inside the particle. Since the objective of these two studies was to look at mass-transfer resistance at the micrograin level, they only considered spherical catalyst fragments, as are typical in an $MgCl_2$-supported catalyst particle.

Simonnazi et al. (1991) in their article appear to have been the first to propose using stress-balance models to describe particle fragmentation and growth. However, they did not actually do so. To the best of our knowledge, the first attempt to model the actual stresses involved in growing polyolefin particles and to relate them to particle morphology was presented by Kittilsen et al. (2001). In that work, a simplified mathematical model related the rate of reaction to the buildup of tension inside the particles in an initial attempt to link chemistry, mass transfer, polymer properties, and particle morphology into a coherent, semipredictive model. It was shown that extremely rapid reactions can indeed lead to a rapid increase in the stress inside the particle, sometimes to a point where the macroparticle will rupture rather than continue to grow homogeneously. In order to examine the particle as in its macroscopic form, the fragmentation process was assumed to happen instantaneously and completely, as for the MGM. In the current article this model is improved and extended to look at how growing catalyst/polymer particles can fragment.

We will concentrate on a rather limited and idealized part of the fragmentation process in this work. The pores are approximated by either an idealized cylindrical shape of uniform size (we will also discuss the effects of pore-size distribution), or other simple geometries. The first part of the article describes a viscoelastic material model for the deposited polymer in cylinders. As will be shown, it is important to consider both the viscous and the elastic nature of the polymer material. Just imagine the different result obtained from crushing a stone by the stroke of a hammer and using a clamp to slowly crush it. The next section shows simulations of polymer growth on cylinder walls, and the resulting stresses in the polymer and in the support material. Finally, we discuss the effects of the different parameters on the breakup process and the polymer particle morphology.

Model Development

The growth of solid polymer inside a catalyst particle results in a change in the local density of the particle (the space

is filled with polymer), and, thus, a localized stress in the material. The fragmentation of the catalyst, and the growth of the polymer particle are governed by the competition between the buildup and relaxation of elastic stresses in the polymer/catalyst particle due to the production of polymer at the active sites. If there is some kind of physical impediment to the expansion of the newly formed polymer, as is the case during the early stages of the polymerization when the particle is essentially composed of a continuous matrix of catalyst support material, the expansion will cause stress in that material. If the stress is larger than the material can stand, it will rupture.

The analysis presented here divides the particle into two phases: catalyst support and polymer. These phases are considered to be pseudohomogeneously distributed throughout the particle. The polymer is assumed to behave as a viscoelastic material, whereas the support material is a pure elastic material. The elastic modulus of the support material is much higher than the polymer, so given the same stress, the strain is much smaller, and is neglected in this context. Thus, the polymer is assumed to grow in a fixed matrix of support material.

Constitutive equations for a viscoelastic material

From the theory of elasticity, the relation between strain and stress is linear, at least for small strains [note that this refers to elastic strains; thus for strains that are relaxed, as will be the case in a viscoelastic material, it is only the elastic part of the strain that must be small ($\ll 1$)]. For an isotropic material this relation is (Boresi and Chong, 1987)

$$\sigma_{\alpha\beta} = \lambda\left(\epsilon_{11} + \epsilon_{22} + \epsilon_{33}\right)\delta_{\alpha\beta} + 2G\epsilon_{\alpha\beta} \tag{1}$$

where λ and G are Lamés elastic coefficients, and δ is the Kronecker delta function. In the analysis that follows, only normal stresses are considered. In the application of the equations, the shear stresses will be zero for symmetry reasons, as will be shown. From Eq. 1 the normal elastic stresses are given as

$$\sigma^e_{ii} = \lambda\left(\epsilon^e_{11} + \epsilon^e_{22} + \epsilon^e_{33}\right)\delta_{\alpha\beta} + 2G\epsilon^e_{ii} \tag{2}$$

$$\sigma^e_{ii} = b\left(\epsilon^e_{jj} + \epsilon^e_{kk}\right)\delta_{\alpha\beta} + a\epsilon^e_{ii} \tag{3}$$

where $a = 2G + \lambda$ and $b = \lambda$ superscript e denotes elastic. Lamés elastic coefficients G and λ are related to Young's modulus, E, Poisson's ratio ν, and the constants a and b as follows

$$G = \frac{E}{2(1+\nu)} \tag{4}$$

$$\lambda = \frac{\nu E}{(1+\nu)(1-2\nu)} \tag{5}$$

$$a = \frac{(1-\nu)E}{(1+\nu)(1-2\nu)} \tag{6}$$

$$b = \frac{\nu E}{(1+\nu)(1-2\nu)} \tag{7}$$

The viscous strain–stress relations are by analogy (White, 1974)

$$\sigma^v_{ii} = \kappa\left(\dot\epsilon^v_{11} + \dot\epsilon^v_{22} + \dot\epsilon^v_{33}\right)\delta_{\alpha\beta} + 2\eta\dot\epsilon^v_{ii} \tag{8}$$

$$\sigma^v_{ii} = \beta\left(\dot\epsilon^v_{ii} + \dot\epsilon^v_{kk}\right) + \alpha\dot\epsilon^v_{ii} \tag{9}$$

where $\alpha = 2\eta + \kappa$ and $\beta = \kappa$, and the dots represent time derivatives. Superscript v denotes viscous.

In this work, the viscoelastic property of the material is modeled by one of the simplest viscoelastic models, the Maxwell model. The model can be envisaged as consisting of a spring and a dashpot in series, or in other words, the total strain is the sum of elastic and viscous strains

$$\epsilon_{ii} = \epsilon^e_{ii} + \epsilon^v_{ii} \tag{10}$$

Now, taking the time derivative of this equation and using Eqs. 3 and 9 results in

$$\dot\epsilon_{ii} = \dot\epsilon^e_{ii} + \dot\epsilon^v_{ii} \tag{11}$$

$$= \left(\frac{\dot\sigma_{ii}}{a} - \frac{b}{a}\left(\dot\epsilon^e_{jj} + \dot\epsilon^e_{kk}\right)\right) + \left(\frac{\dot\sigma_{ii}}{\alpha} - \frac{\beta}{\alpha}\left(\dot\epsilon^v_{jj} + \dot\epsilon^v_{kk}\right)\right) \tag{12}$$

$$\Rightarrow \dot\sigma_{ii} = b\left(\dot\epsilon_{jj} + \dot\epsilon_{kk}\right) + a\dot\epsilon_{ii} - \frac{a}{\alpha}\sigma_{ii} \tag{13}$$

The last step is valid only if $\alpha/\beta = a/b$. This is validated by examining pure elastic materials, where the following relation holds

$$\frac{a}{b} = \frac{1-\nu}{\nu} \tag{14}$$

Thus, a/b is a pure function of Poisson's ratio ν, which is the ratio of the lateral contracting strain to the elongational strain when a rod is stretched by a force applied at its ends. We assume the viscous part of the model behaves in the same manner, and, thus, $\alpha/\beta = a/b$.

The bulk viscosity κ in viscous fluids is often an unknown parameter. Stoke has assumed that it equals $2/3\eta$, and the same has also been proven valid for monatomic gases. However, there is a dispute whether the proof holds (White, 1974). Given our assumption that $\alpha/\beta = a/b$, and setting $\kappa = 2/3\eta$ means that Poisson's ratio becomes $\nu = 1/3$, a value in the middle of the range for most materials. Most fluids are assumed incompressible in fluid-dynamic calculations, in which cases the bulk viscosity is irrelevant.

In further analysis it is assumed that the changes taking place are performed such that the material is always in a pseudo steady-state. This is valid as long as the changes in the strain rates are slow compared to the changes in the stresses, that is, no acceleration is taking place. Then, at all times, the stresses must balance. The momentum balance is then simply

$$\nabla\cdot\boldsymbol{T} = 0 \tag{15}$$

where the total stress tensor can be decomposed into contributions from pressure and stress as

$$\mathbf{T} = -\mathbf{I}\cdot p + \boldsymbol{\sigma} \tag{16}$$

Furthermore, it is assumed that no significant pressure gradient is in the shell. The moment balance then becomes

$$\nabla \cdot \boldsymbol{\sigma} = 0 \tag{17}$$

When the coordinate system is fixed in time, taking the time derivative of the moment balance yields

$$\frac{\partial}{\partial t} \nabla \cdot \boldsymbol{\sigma} = \nabla \cdot \boldsymbol{\sigma} = 0 \tag{18}$$

Thus, both the instantaneous (Eq. 17) and the time derivative of the stresses (Eq. 18) must fulfill the moment balance.

The general viscoelastic strain–stress equation (Eq. 13) can be envisaged as being a difference of an elastic stress and the total stress

$$\dot{\sigma}_{ii} = \dot{\sigma}_{ii}^{e} - \frac{a}{\alpha} \sigma_{ii} \tag{19}$$

where σ_{ii}^{e} is the elastic stress in a pure elastic material given the present strains (compare this last equation with Eq. 13. Inserting the vector form of this into Eq. 18, yields

$$\nabla \cdot \left(\dot{\boldsymbol{\sigma}}^{e} - \frac{a}{\alpha} \boldsymbol{\sigma} \right) = 0 \tag{20}$$

$$\Rightarrow \nabla \cdot \dot{\boldsymbol{\sigma}}^{e} - \frac{a}{\alpha} \nabla \cdot \boldsymbol{\sigma} = 0 \tag{21}$$

$$\nabla \cdot \dot{\boldsymbol{\sigma}}^{e} = 0 \tag{22}$$

$$\nabla \cdot \boldsymbol{\sigma}^{e} = C \tag{23}$$

where C is a constant. The step from Eq. 16 to Eq. 22 is valid by using $\nabla \cdot \boldsymbol{\sigma} = 0$ (Eq. 17). The last step is obtained by taking the time derivative outside the spatial derivative, which is possible with a time-fixed coordinate system. When solving the model presented here, it is Eq. 22 that is the key. It is difficult to solve this directly. However, it is possible by first solving Eq. 23 with the constant $\boldsymbol{C} = 0$, then taking the time derivative. This is the same as solving a steady-state pure elastic case. The solution with $\boldsymbol{C} = 0$ is valid because a constant term in this equation will only add a constant to the displacement function (see Eqs. 24, 32, and 33) that will disappear when taking the time derivative. All together this means that the solution of the pure elastic case is of vital importance.

Pure elastic compression of a cylinder shell

Assuming cylindrical symmetry, all off-diagonal terms in the stress tensor cancel, and the equations of momentum reduce to only one (Bird et al., 1960)

$$\frac{1}{r} \frac{d}{dr} (r \sigma_r) - \frac{\sigma_t}{r} = 0 \tag{24}$$

where σ_r is the radial component of the global stress vector (= the diagonal of the $\boldsymbol{\sigma}$ tensor), and σ_t equals the tangential component. From Eq. 3, the elastic stress–strain relations are

$$\sigma_r = a \epsilon_r + b \epsilon_t \tag{25}$$

$$\sigma_t = a \epsilon_t + b \epsilon_r \tag{26}$$

In order to solve the momentum balance, a displacement function is introduced. It tracks the displacement of single infinitely small control volumes as a function of the original radial position (radial position before the deformation takes place). It is defined as

$$U = \rho(r) - r \tag{27}$$

where ρ is the position after deformation of the point originally located at r. The radial and tangential deformations are expressed in terms of this function as

$$\epsilon_r = \frac{[\rho(r + dr) - \rho(r)] - dr}{dr} = \frac{d\rho}{dr} - 1 = \frac{dU}{dr} \tag{28}$$

$$\epsilon_t = \frac{2\pi\rho - 2\pi r}{2\pi r} = \frac{\rho - r}{r} = \frac{U}{r} \tag{29}$$

Substituting these relations into Eqs. 25 and 27, yields

$$\sigma_r = a \frac{dU}{dr} + b \frac{U}{r} \tag{30}$$

$$\sigma_t = b \frac{dU}{dr} + a \frac{U}{r} \tag{31}$$

Further substituting these relations into the momentum balance Eq. 24, we obtain

$$\frac{d^2U}{dr^2} + \frac{1}{r} \frac{dU}{dr} - \frac{U}{r^2} - 0 \tag{32}$$

Integration results in

$$U = C_1 r + \frac{C_2}{r} \tag{33}$$

where C_1 and C_2 are constants determined by boundary conditions.

Two cases are considered in which results are important for the further development of the model. First is the compression of a cylinder shell with original inner radius r_i and original outer radius r_p. At the inner and outer boundary of the polymer shell, stresses must balance. It is assumed there is no difference in pressure inside and outside the polymer shell, which means that the external (applied) and internal (in the material) must balance. At the outer surface, stress is applied in such manner that this outer surface is displaced by $-\Delta w$. No external stress acts at the inner surface. The boundary conditions are thus

$$r = r_p, \qquad U = -\Delta w \tag{34}$$

$$r = r_i, \qquad \sigma_r = 0 \tag{35}$$

Using these boundary conditions, the displacement function becomes [N.B., using the expressions for a and b in Eqs. 6 and 7, it can be shown that $(a-b)/(a+b)=1-2\nu$)

$$U=-\Delta w\frac{\left(\frac{a-b}{a+br}\frac{r}{r_i}+\frac{r_i}{r}\right)}{\left(\frac{a-b}{a+b}\frac{r_p}{r_i}+\frac{r_i}{r_p}\right)} \tag{36}$$

$$=-\Delta w\frac{\left((1-2\nu)\frac{r}{r_i}+\frac{r_i}{r}\right)}{\left((1-2\nu)\frac{r_p}{r_i}+\frac{r_i}{r_p}\right)} \tag{37}$$

The second case to study is an elastic compression of a cylinder shell where the inner radius is fixed and the stress at this surface is given. The boundary conditions for this case are

$$r=r_p,\quad \begin{cases} U=0 \\ \sigma_r=\sigma_r^w \end{cases} \tag{38}$$

The displacement function is solved using these boundary conditions. The solution is

$$U=\frac{\sigma_r^w r_p}{2a}\left(\frac{r}{r_p}-\frac{r_p}{r}\right) \tag{39}$$

Viscoelastic model of polymer growing on the inside of a cylinder

The specific process to model is of that of the buildup of the viscoelastic stresses in the polymer and on the cylinder wall during deposition (growth) of polymer on the inside of a pore wall (here likened to a cylinder). In the preceding sections, all necessary equations to describe this are given. These are merged together in this section.

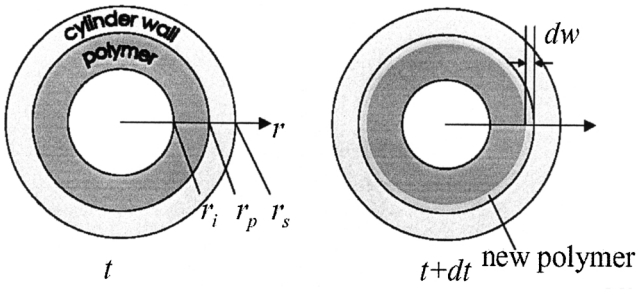

Figure 1. Deposition of polymer on the inside of a cylindrical pore.

The left figure shows the situation at time t, where the polymer cylinder has an inner radius r_i and an outer radius r_p. During the time dt, a small amount of new polymer is formed (lighter color) underneath the polymer already deposited. The width of the new polymer shell is dw. As the new polymer is deposited, the inner radius r_i of the cylinder shell decreases.

The growth of the polymer is shown in Figure 1. In a short time period, dt, an amount of polymer, dV, is formed in a pore ($dV \propto Rdt$). In a case with no stress this would make a shell of radius r_p, length L, and width dw ($dV=2\pi r_p dwL$). The presence of the stress will make the shell somewhat compressed, and, thus, thinner. This effect is normally negligible since it can be shown that the strain will be $\epsilon_r=\sigma_r^w/a$, which for all practical purposes is much smaller than 1.

The growth process, inserting the slice with thickness dw, can be studied by regarding the process as an elastic compression, then calculating the change in the stress according to the viscous effects. The use of pure elastic displacement in this context was validated in Eqs. 20–23.

The displacement of the polymer existing before inserting the slice dw at $r=r_p$ can be found using the results from an elastic compression of a cylinder given in Eq. 37. The displacement function at time t for the time interval dt is given as

$$dU(r,t)=-dw(t)\frac{\left((1-2\nu)\frac{r}{r_i(t)}+\frac{r_i(t)}{r}\right)}{\left((1-2\nu)\frac{r_p}{r_i(t)}+\frac{r_i(t)}{r_p}\right)} \tag{40}$$

so

$$\frac{\partial U(r,t)}{\partial t}=-\frac{dw(t)}{dt}\frac{\left((1-2\nu)\frac{r}{r_i(t)}+\frac{r_i(t)}{r}\right)}{\left((1-2\nu)\frac{r_p}{r_i(t)}+\frac{r_i(t)}{r_p}\right)} \tag{41}$$

where r refers to the position in the shell before inserting the cylinder slice dw. Using the preceding result, it is now possible to calculate the time derivative of the elastic stresses

$$\dot{\sigma}_r^e=\frac{\partial\sigma_r^e}{\partial t}=a\frac{\partial}{\partial r}\left(\frac{\partial U}{\partial t}\right)+\frac{b}{r}\frac{\partial U}{\partial t} \tag{42}$$

$$\dot{\sigma}_t^e=\frac{\partial\sigma_t^e}{\partial t}=b\frac{\partial}{\partial r}\left(\frac{\partial U}{\partial t}\right)+\frac{a}{r}\frac{\partial U}{\partial t} \tag{43}$$

The necessary expressions are

$$\frac{\partial}{\partial r}\left(\frac{\partial U}{\partial t}\right)=-\frac{dw(t)}{dt}\frac{\left((1-2\nu)\frac{1}{r_i(t)}+\frac{r_i(t)}{r^2}\right)}{\left((1-2\nu)\frac{r_p}{r_i(t)}+\frac{r_i(t)}{r_p}\right)} \tag{44}$$

$$\frac{1}{r}\frac{\partial U}{\partial t}=-\frac{dw(t)}{dt}\frac{\left((1-2\nu)\frac{1}{r_i(t)}+\frac{r_i(t)}{r^2}\right)}{\left((1-2\nu)\frac{r_p}{r_i(t)}+\frac{r_i(t)}{r_p}\right)} \tag{45}$$

The time derivatives of the elastic stresses are then

$$\dot{\sigma}_r^{\,e}(r,t) = -\frac{dw}{dt}(a-b)\frac{\dfrac{1}{r_i(t)} - \dfrac{r_i(t)}{r^2}}{(1-2\nu)\dfrac{r_p}{r_i(t)} + \dfrac{r_i(t)}{r_p}} \tag{46}$$

$$\dot{\sigma}_t^{\,e}(r,t) = -\frac{dw}{dt}(a-b)\frac{\dfrac{1}{r_i(t)} + \dfrac{r_i(t)}{r^2}}{(1-2\nu)\dfrac{r_p}{r_i(t)} + \dfrac{r_i(t)}{r_p}} \tag{47}$$

Now we can insert these results into Eq. 19 to obtain the necessary viscoelastic model. For a symmetric cylinder, Eq. 19 becomes

$$\dot{\sigma}_r = \dot{\sigma}_r^{\,e} - \frac{a}{\alpha}\sigma_r \tag{48}$$

$$\dot{\sigma}_t = \dot{\sigma}_t^{\,e} - \frac{a}{\alpha}\sigma_t \tag{49}$$

where $\dot{\boldsymbol{\sigma}}^{\,e}(r,t)$ can be taken from Eqs. 46 and 47. Note that r is the radius in a time-fixed coordinate system, and that the equations are valid for the polymer in $r_i < r < r_p$.

The last obstacle is the boundary condition. The displacement in the inserted slice with width dw is equivalent to the displacement in the case outlined in Eqs. 38 and 39. Using these relations, the radial and tangential strains in the slice are

$$\epsilon_r = \frac{dU}{dt} = \frac{\sigma_r^{\,w} r_p}{2a}\left(\frac{1}{r_p} + \frac{r_p}{r^2}\right) \tag{50}$$

$$\epsilon_t = \frac{U}{r} = \frac{\sigma_r^{\,w} r_p}{2a}\left(\frac{1}{r_p} - \frac{r_p}{r^2}\right) \tag{51}$$

The stresses are

$$\sigma_r = \frac{\sigma_r^{\,w} r_p}{2}\left(\left(1+\frac{b}{a}\right)\frac{1}{r_p} + \left(1-\frac{b}{a}\right)\frac{r_p}{r^2}\right) \tag{52}$$

$$\sigma_t = \frac{\sigma_r^{\,w} r_p}{2}\left(\left(1+\frac{b}{a}\right)\frac{1}{r_p} - \left(1-\frac{b}{a}\right)\frac{r_p}{r^2}\right) \tag{53}$$

Using the first of these relations, the derivative of the radial stress is

$$\frac{\partial \sigma_r}{\partial r} = -\frac{\sigma_r^{\,w} r_p^2}{r^3}\left(1-\frac{b}{a}\right) \tag{54}$$

The conditions on the outside of the inserted slice are needed. This corresponds to inserting $r = r_p + dw$ in the previous equations. As $dw \to 0$, it is equivalent to inserting $r = r_p$. Thus

$$\left.\frac{\partial \sigma_r}{\partial r}\right|_{r_p} = -\frac{\partial_r^{\,w}}{r_p}\left(1-\frac{b}{a}\right) \tag{55}$$

$$\sigma_t|_{r_p} = \frac{b}{a}\sigma_r^{\,w} \tag{56}$$

The boundary conditions for the model can then be summarized as

$$t = 0, \qquad \forall r \begin{cases} \sigma_r(r) = 0 \\ \sigma_t(r) = 0 \\ r_i = r_p \end{cases} \tag{57}$$

$$t > 0, \qquad r = r_p \begin{cases} \dfrac{\partial \sigma_r}{\partial r} = -\dfrac{\sigma_r(r_p)}{r_p}\left(1-\dfrac{b}{a}\right) \\ \sigma_t = \dfrac{b}{a}\sigma_r(r_p) \end{cases} \tag{58}$$

For the purpose of examining which parameters are important for the stress, it is convenient to transform the variables into a set of dimensionless parameters

$$t' = \frac{t}{\tau} \tag{59}$$

$$r' = \frac{r}{r_p} \tag{60}$$

$$\sigma' = \frac{\sigma}{G} \tag{61}$$

where

$$\tau = \frac{\alpha}{a} = \frac{\eta}{G} \tag{62}$$

where τ is often called the relaxation time. Using these parameters, and the relations between a and b, and ν and G (Eqs. 4–7), the elastic stress equation (Eq. 46) can be written in dimensionless form as

$$\frac{\partial \sigma_r^{\,e\prime}}{\partial t'} = -2R'_\nu f_r(r', r'_i, \nu) \tag{63}$$

where

$$R'_\nu = \frac{dw}{dt}\frac{\tau}{r_p} = R_\nu \frac{\tau}{r_p} \tag{64}$$

and

$$f_r(r', r'_i, \nu) = \frac{\dfrac{1}{r'_i} - \dfrac{r'_i}{r'^2}}{(1-2\nu)\dfrac{1}{r'_i} + r'_i} \tag{65}$$

Now, introducing the preceding dimensionless parameters into the total stress equation (Eq. 48), this can be written as

$$\frac{\partial \sigma_r'}{\partial t'} = -2R_v' f_r(r', r_i', \nu) - \sigma_r' \tag{66}$$

An analogous equation can be set up for the tangential stress, replacing f_r with a similar function f_t

$$f_t(r', r_i', \nu) = \frac{\dfrac{1}{r_i'} + \dfrac{r_i'}{r'^2}}{(1-2\nu)\dfrac{1}{r_i'} + r_i'} \tag{67}$$

Numerical solution

The numerical solution of the problem treated in the preceding sections is explained below. The discretizing scheme is shown in Figure 2, and can be summarized as follows:

- At a time t the polymer shell is discretized, evenly distributing n nodes from the inner r_i to the outer radius r_p.
- After a time dt, a shell of width dw is placed at r_p between the polymer already there and the support wall at radius r_p.
- The new positions of the n nodes are found using the displacement function dU given in Eq. 40.
- The stresses at the n nodes in the "old" polymer are updated according to Eqs. 46 and 47.
- The stress in the new polymer at r_p is related to the "old" polymer by Eqs. 55 and 56 giving the position (r_p) and stress at a new node. Thus, at time $t + dt$ the stresses at $n+1$ nodes are known.
- Before the next time step the polymer shell is rediscretized into n nodes by interpolating from the present $n+1$ nodes. In this way, at every time step the stresses in the n nodes that are evenly distributed in the polymer shell will be known.

Stress in the catalyst support

The preceding derivation was for the stress in the polymer material. The catalyst support making the solid wall in the cylinder was treated only as a nonelastic material, giving the boundary condition $U(r_p) = 0$. In reality, the catalyst support breaks during the fragmentation of the catalyst particle. Thus, it is essential to examine the stress in the catalyst support. This is shown in this section.

In a real catalyst particle, there is a wide distribution of pore sizes and thickness of support walls between the pores. In this first analysis, only a very simple case is shown. The results will be illustrative, but not necessarily 100% quantitative. The model used in this section is a cylindrical pore surrounded by support material, but with no interaction with other pores. In reality, the catalyst support forms a continuous structure within the catalyst particle. The results obtained below will be an estimate of the average stress in the support. The support is assumed to be purely elastic. The interesting quantity in this case is the tangential stress. The material will break when this stress exceeds a critical limit.

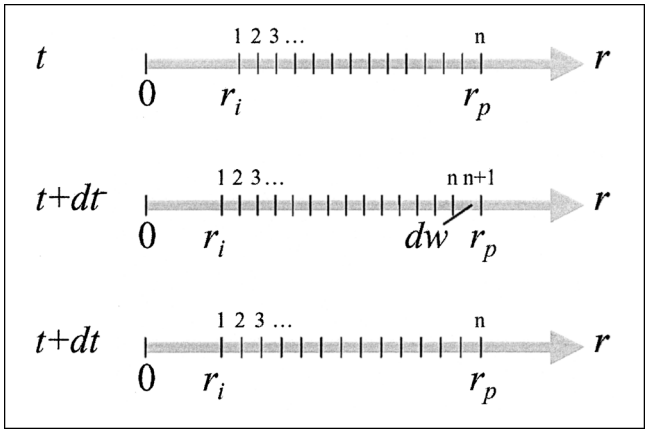

Figure 2. Discretizing scheme in the numerical solution.

As in the previous sections, a steady-state analysis is done. The moment balance for the support is taken, and a solution in terms of a displacement function is similar to Eq. 33. The boundary conditions for the support are

$$r = r_p, \qquad \sigma_r^s = -\sigma_r^w \tag{68}$$

$$r = r_s, \qquad \sigma_r^s = 0 \tag{69}$$

where r_p is the radius of the pore (and inner radius of the support cylinder shell) and r_s is the outer radius of the support cylinder shell. The first boundary condition is a result of the stress balance at the interface with the polymer. Eliminating the constants of the general solution (Eq. 33) using the boundary conditions and a general constitutive equation for an elastic material, the tangential stress is

$$\sigma_t^s = -\sigma_r^w \frac{\left(1 + \dfrac{r_s}{r}\right)^2}{1 - \left(\dfrac{r_s}{r_p}\right)^2} \tag{70}$$

Taking the area average of the tangential stress over the cross section of the cylinder shell results in

$$\bar{\sigma}_t^s = \frac{-\sigma_r^w}{1 - \left(\dfrac{r_s}{r_p}\right)^2}\left(1 + \frac{2\ln\dfrac{r_s}{r_p}}{1 - \left(\dfrac{r_p}{r_s}\right)^2}\right) \tag{71}$$

where r_s can be expressed in terms of the void fraction of the catalyst particle. The relation is given by

$$\epsilon_0 = \frac{r_p^2}{r_s^2 - r_p^2} \tag{72}$$

$$\Rightarrow \frac{r_p}{r_s} = \sqrt{\frac{\epsilon_0}{1+\epsilon_0}} \tag{73}$$

Reaction rate and specific surface area in the catalyst

One of the key parameters in the model just presented is the rate of polymerization, in terms of $R_v = dw/dt$. This is related to more generally known terms in this section.

One common way of representing the activity in olefin polymerization is in terms of the mass of polymer per mass of catalyst and time. We can envisage R_v as representing the velocity of the polymer away from the active surface. Thus, the specific surface area must be estimated.

Using the principles of the model presented in the previous sections, we can estimate the specific surface as the inner radius of the cylinder pore to the volume of the cylinder. This is

$$A = \frac{2\pi r_p L}{\pi r_s^2 L} = 2\frac{r_p}{r_s} \tag{74}$$

Expressing the cylinder radius r_s by the void fraction (Eq. 73), the preceding equation can be rewritten

$$A = \frac{2\epsilon_0}{(1+\epsilon_0) r_p} \tag{75}$$

Another common way of expressing the surface area is in terms of area per unit mass

$$A' = \frac{2\epsilon_0}{(1-\epsilon_0)(1+\epsilon_0)\rho_c r_p} \tag{76}$$

where ρ_c is the density of the support material. Using common parameter values (see Table 1), the specific surface area is set to 2.0×10^5 m^2/kg.

The relation between R_v and the reaction rate R_m (in kg/kg/h) is

$$R_v = \frac{\dfrac{R_m}{3{,}600 s/h\, \rho_p}}{A'} \tag{77}$$

$$R_v = \frac{1}{7{,}200 s/h} \frac{(1-\epsilon_0)(1+\epsilon_0)}{\epsilon_0} \frac{\rho_c}{\rho_p} r_p R_m \tag{78}$$

The reaction rate as a function of time is given by

$$R = R_0\left[1-\exp(-t/\tau_k)\right] d(t) \tag{79}$$

where R_0 is the peak activity, τ_k is the kinetic time constant, and $d(t)$ is a deactivation function. For $t \ll \tau_k$, deactivation is not important, and the exponential function can be approximated by a linear relationship, and the reaction rate can be equivalently written as

$$R = R_0 t/\tau_k \tag{80}$$

Results and Discussions

Base-case parameters

Precise parameters for the systems described in this work were hard to find. The most relevant data were found for the polymerization of ethene on silica support. The model characteristics are illustrated mainly using order-of-magnitude parameter values. This is an appropriate approach given that the parameters vary greatly with type of support, polymer, and reaction conditions. The base-case parameters are listed in Table 1.

The polymer elastic modulus was kindly supported by Borealis AS (Borealis, personal communication to P. K., 2001) based on standard elongation tests at reaction temperatures $T = 80$°C, in air. The parameter value for the viscosity was based on the data by Gao and Mackley (1994), which is also used in the work by Agarwal (1998). The parameter value for the viscosity was for UHMWPE at $T = 135$°C. This polymer showed relaxation times on the order of 0.3 to 1.3 s, but for very high content of solvent. Extrapolating back to zero solvent concentration gives relaxation times of 1–100. Based on this, the viscosity is set relative to the elasticity with a relaxation time of 10. Poisson's ratio ν was set to 0.45. According to van Krevelin (1990), the Poisson ratio is about 0.42–0.49 for polyethene (an incompressible material has $\nu = 0.5$).

In the simulations with the base-case parameters and in the parameter sensitivity analysis, a constant reaction rate was used. This was set in such a manner that the pore would fill (and break) with polymer in 5 s if the polymer was incompressible. This time scale is in accordance with the expected time scale for particle rupture. Thus, $R_v/r_p = 0.1$ s^{-1}, corresponding to $R_m = 680$ kg/kg/h, given the base-case parameters. This reaction rate is typical for the very first part of the polymerization and should not be confused with the normal maximum activity for modern catalysts (10,000 to 100,000 kg/kg/h). A more realistic activity relation is used in the

Table 1. Base-Case Parameters for Polymerization of Polyethene at $T = 80$°C

Parameter	Symbol	Value	Units	Reference
Pore radius	r_p	10^{-8}	M	Estanoz and Chiovetta (1996)
Initial porosity	ϵ_0	0.8		Estanoz and Chiovetta (1996)
Support density	ρ_c	2,250	kg/m^3	Estanoz and Chiovetta (1996)
Polymer density	ρ_p	950	kg/m^3	Jastrzebski (1987)
Elasticity	G	10^8	Pa	Borealis (personal communication to P. K., 2001)
Viscosity	η	10^9	Pa·s	Gao and Mackley (1994)
Poisson's ratio	ν	0.45		Van Krevlin (1990)
Reaction rate	R_v	10^{-9}	m/s	Corresponds to 680 kg PE/kg Cat/h
Kinetic time constant	τ_k	100	S	Kittilsen et al. (2001)
Peak activity	R_0	10^2–10^5	kg/kg/h	Kittilsen et al. (2001)
Critical support stress	σ_c^s	$3\cdot10^7$	Pa	Adjustable

"Particle Morphology" section; the rate starts at zero and increases exponentially with the kinetic time constant τ_k and the peak activity R_0. Finally, the critical stress for breaking the support material used in the morphology study was adjusted to give reasonable final morphologies in the simulations. Actual critical stress data for silica will be difficult to use, because small imperfections and cavities in the material will have a strong impact on the critical stress.

Simulations with base-case parameters

The model was solved using the base-case parameters for the time interval 0 to 5 s. The amount of polymer made in this time would fill up the pores if the polymer was incompressible and inviscid, given the reaction rate and pore size defined as base-case parameters. The calculated radial and tangential stresses as a function of position in the polymer shell are shown in Figure 3.

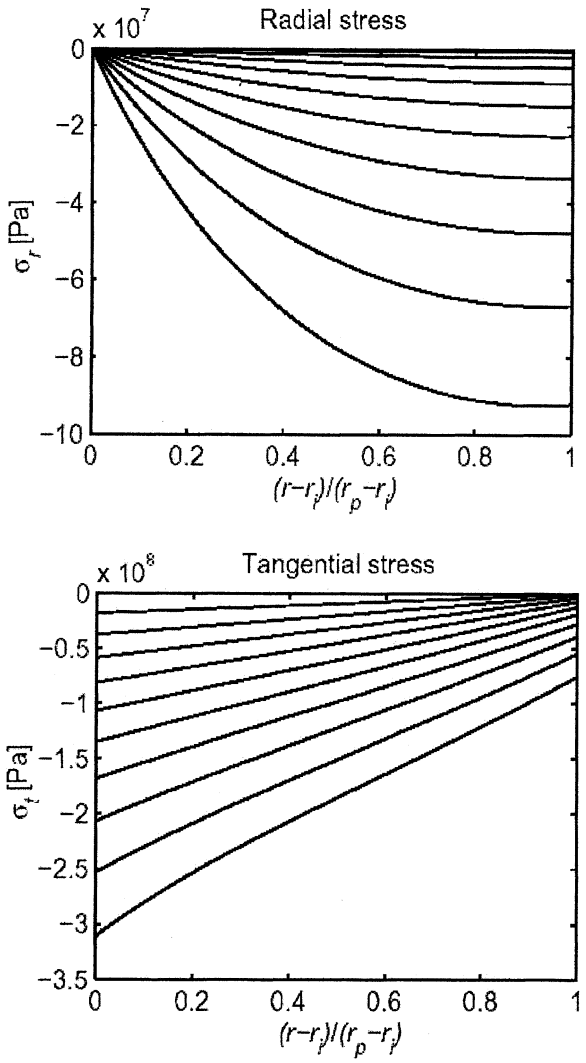

Figure 3. Radial stress (top) and tangential stress (bottom) in the polymer shell as a function of position and time.

The step in time is evenly distributed from $t = 0$ to $t = 5$ s; the lower curves are for larger times. The x-axis is scaled in such a manner that it runs from the inner to the outer radius of the polymer shell, with a scale relative to the width of the shell.

Both absolute values of radial and tangential stresses increase with time (and amount of polymer deposited) as expected. Both are negative, indicating a compressive stress. The tangential stress is at its absolute maximum at the inner radius, r_i, of the polymer shell. Obviously, this part of the shell has gone through the largest compressive strain, and, therefore, has the largest tangential stress. The radial stress is at its absolute maximum near the pore surface, r_p. New polymer is continuously added at the pore surface. Within a short time interval a new shell of polymer is squeezed in between the pore wall and the already existing polymer. This new polymer shell will have a slightly larger outer surface than inner surface. Applying a given stress at the outer surface of this shell will result in a larger stress at the inner surface of the new shell (Eq. 52). Second, due to the free surface at the inner surface of the total polymer shell, the radial stress must approach zero there. Thus, there will be an absolute maximum stress near the cylinder wall.

From a morphological point of view, the most interesting stress to consider is the radial stress at the pore wall, at $r = r_p$ [that is, at $(r - r_i)/(r_p - r_i) = 1$]. If the support does not break, this radial stress must be counterbalanced by an equally large radial stress in the support material, and is, thus, the stress that will determine whether the support will rupture or stand the production of even more polymer in the pore. This will be further analyzed in the "Morphology" section below.

To illustrate the rate of pores filling, inner radius of the polymer shell as a function of time is plotted in Figure 4. The base-case parameters are used. The inner radius follows an almost linear relation with time, meaning that the inner parts of the shell have been significantly compressed. In this case, the inner radius at $t = 5$ s is $r_i = 0.36 r_p$, corresponding to a porosity of $r_p = 0.13$. This porosity means that the density of

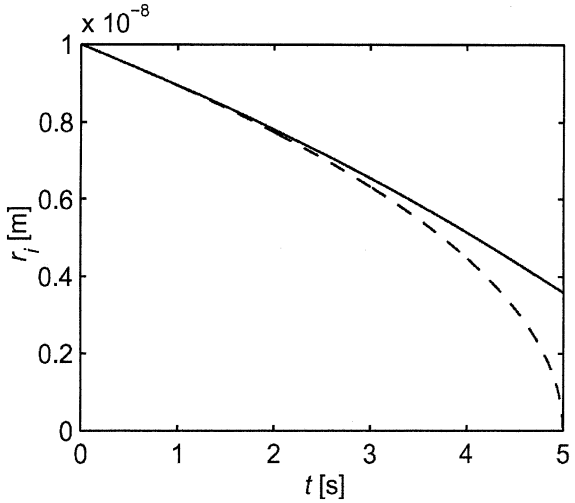

Figure 4. Inner radius r_i of a compressible polymer shell as a function of time.

The base-case parameters are used. The dashed line shows the situation if the material was incompressible, in which case the pore would have filled up at time $t = 5$ s.

the compressed polymer is about 15% higher than in an incompressible case.

Parameter sensitivity

As can be seen from the dimensionless model (Eq. 66), two parameters determine the dimensionless stress as a function of dimensionless time and position, namely, the reaction rate R_v and Poisson's ratio ν. $R'_v = \tau/(r_p/R_v)$ can be regarded as the relative time scale of the relaxation of the stresses (τ) and the filling of the pore (r_p/R_v). Thus, $R'_v \gg 1$ means fast filling compared to the relaxation of the stresses. Then, the stresses become mainly elastic; $R'_v \ll 1$ means that the stresses will be relaxed because of viscous displacement in the material. The other parameter, ν does not have an important effect as long as it is not very close to the critical value of 0.5, corresponding to an incompressible material (see Figure 4). For most polymers this parameter does not vary much, and is thus not discussed further here.

The effects on the radial stress (at the pore wall) with three different values of R'_v are shown in Figure 5. The time is scaled to make it easy to compare the three cases, dividing by the time it would take to fill the pore if the polymer were incompressible. In other words, $t_{\text{fill}} = r_p/(2R_v)$.

For $R'_v = 10$, the stress develops fastest. There is little time for relaxation of the stress. Instead, for $R'_v = 0.10$, the reaction is slow enough for the stress to relax somewhat during growth. Thus, the stress at the same degree of filling will be smaller. The balance between the buildup and relaxation of stresses will be important for the development of the morphology, as is discussed next.

Particle morphology

As mentioned in the Introduction, the final particle morphology is, to a large extent, determined by the morphology of the fragmented catalyst particle. The preceding sections demonstrated how the stress in the polymer, and more importantly for the morphology, the stress at the support–polymer interface varied with reaction conditions. This is discussed more in detail here.

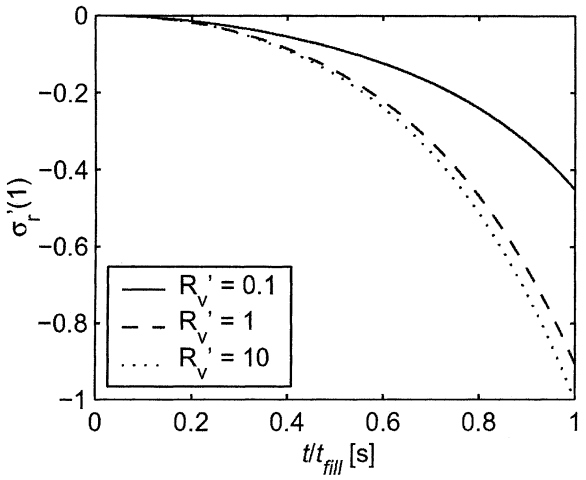

Figure 5. Demonstration of model sensitivity to dimensionless reactivity R'_v.

The radial stress at $r' = 1$, corresponding to the radial stress at the support wall, is shown as a function of reaction time t divided by the filling time for an incompressible polymer t_{fill} given the same R'_v.

Effect of Polymer Physical Properties and Reaction Rate. Generally, it can be stated that all parameters that make the stress in the polymer greater for a given polymer production will increase the porosity of the fragmented particle. Also, all parameters that lower the critical stress for breakup of the support will make the particle more porous.

As we have seen, increasing the reaction rate will result in less time for relaxation of the stress, and, thus, rupture at a lower degree of filling, that is, higher porosity with increasing reaction rate. This can be one of the factors explaining the observation of Weickert et al. (1999), who found that upon increasing the reaction rate, the polymer particles became more porous and fine in structure.

Similar to increasing the reaction rate, decreasing the viscosity of the polymer (that is, lowering the relaxation time, τ), will decrease the porosity (as long as the polymer has not melted). The effect of these two parameters is shown in Figure 6, where the porosity at the rupture is plotted as a function of reaction rate for different relaxation times. These results were obtained using the base-case parameters and a realistic catalyst activity with time from Eq. 80. Also shown in this figure is the time it takes for the particle to rupture. Comparing this time with the relaxation time helps to explain the different behaviors at different relaxation times. The cases with the shortest relaxation times have more time to relax the stress before rupture, which means that the catalyst particle can generate more polymer in the same volume before fragmentation, and the porosity is, therefore, lower.

Effect of Support Properties. As long as the support does not break, the force exerted by the growing polymer on the support is counterbalanced by a force of equal magnitude from the support. This, of course, is the source of stress in the support material, and can eventually cause the support to break, if raised above the critical stress the support can stand. An estimate of the stress in the support as a function of the stress exerted on the interface was given in Eq. 71. Together with the equation relating the radius of the pores and support to the initial porosity (see Eq. 73), this is our basis for describing the rupture of the catalyst.

Obviously, all effects that cause a reduction in the critical stress of the support will make a more porous particle. In the extreme case, where the particle support fragments before enough polymer exists to hold the fragments together, the original particle can disintegrate. Such effects can be small physical or chemical imperfections in the support material, or be provoked by the shape and distribution of the pores, as discussed below.

It is reasonable to assume that the initial porosity of the initial catalyst support plays some role in determining the porosity of the final polymer particle. It is possible that the relationship between the initial and final porosities is not at all linear. A particle with low initial porosity will have more support (or thicker pore walls) and smaller pores. Less stress will be generated in these smaller pores compared to a more porous particle. Furthermore, since the pore walls are thicker in the less porous particles, they will probably fragment later. In other words, raising the porosity of a support particle will raise the porosity of the final polymer particle even more.

The effect of changing pore size is an important issue. Let us compare two particles: one containing large pores, and one containing small pores. The porosity is set to the same value and the reactivity is set to the same level in terms of activity per area (R_v is the same). Then, R'_v, and, thus, the interface stress will be smallest for the particle containing the largest pore. Because the porosity is the same, Eqs. 71 and 73 show that the stress in the support will be lower and have larger pores. However, studies presented in the literature report processes starting by fragmentation in the larger pores, then successively continuing with the smaller pores (for example, Ferrero et al., 1992a; Estenoz and Chiovetta, 1996; Pater, 2001). Of course, these studies were done with particles having a particle-size distribution, so that small and large pores are located in the same particle. In that case, a more correct point of view is to consider the pores "seeing" different porosities. What is relevant for the fragmentation is how much support material the pore has to break. Thus, the relevant porosity for the largest pores, ranging in the macro level of the particle, is the macroporosity, or approximately the total porosity of the particle. For the smallest pores, the local porosity will be the porosity of the particle when not including the macropores, so it will be much smaller. This means that the smallest pores are surrounded by more support than the macropores. Even though the stress at the polymer–support interface is smaller for the largest pores, the total surface compared to the amount of support to break is less than with smaller pores. Thus, it is natural that in a particle with different pore sizes, the largest pores will break first, then smaller and smaller pores reach the critical limit for rupture.

Pore shape might also be important. For instance, another effect that makes the larger pores break first is the "crowbar effect" that appears when the pores are more conic shaped than the idealized cylinders considered in this work. Conic-shaped pores will have a critical point at the top of the cone top. Stress at the cone walls will act with a momentum at this point. Large pores will have a much larger total surface compared to small pores, and, thus, the total momentum at the critical point will be larger, even though the stress at the surface is the same. An illustration of this effect is shown in Figure 7. The general elastic stress–strain equations were solved for a 2-D case where the same stress was applied to the surfaces of two different V-shaped holes in a block of an elastic material. It clearly illustrates that even if the stresses at the surfaces are the same, the largest pore results in a much larger stress at the critical point. This last result is interesting, since it helps us to quantitatively understand how fragmentation of the support takes place, and lends credence to the idea that particles fragment successively on the largest pores, followed by medium-sized pores, and so on, rather than on a layer-by-layer basis. This is probably true for $MgCl_2$-supported particles, as well as for silica particles. The former simply fragment faster because of the nature of the support.

Conclusions

A new viscoelastic model to describe the fragmentation process of olefin polymerization catalyst particles was developed and demonstrated. Idealized, equal-sized cylindrical and triangular pores were considered. The polymer produced inside of these pores causes stress to form in the polymer, which is in turn transmitted to the support. Because polymer is a viscoelastic material, the polymer formed will deform and the stress will be somewhat relaxed with time. Thus, one of the key parameters is the rate of reaction compared to the relaxation time of the polymer. In turn, it is possible that the relaxation time is affected by the rate of crystallization of the nascent polymer, local temperatures, and swelling conditions in the polymer. The model allows us to conclude that:

- The viscoelastic model can explain variation in porosity with activity. Fast reaction means less relaxation of stress and faster rupture, and, thus, higher porosity at rupture.
- All factors that increase the relaxation time of the polymer, that is, make the polymer more viscous, will produce less porosity. This can be caused by chemical (such as comonomer addition) or physical (such as the presence of a swelling agent) changes in the polymer.
- All factors that reduce the critical stress the support can stand will make a more porous polymer. Such factors can be

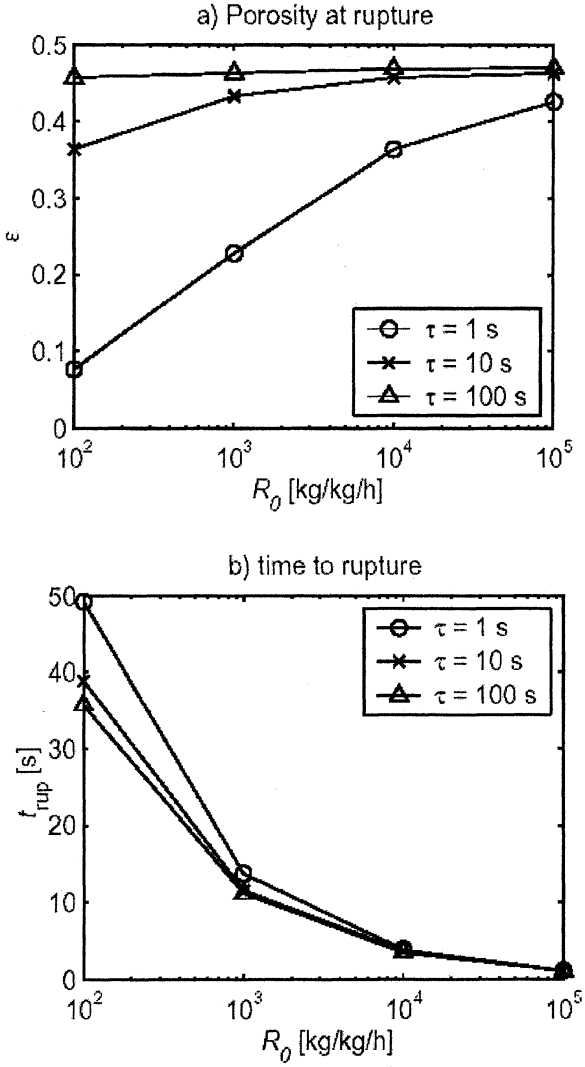

Figure 6. Effect on particle porosity at rupture as a function of peak activity, R_0, for different relaxation times $\tau = \eta/G$.

small physical or chemical imperfections in the support material.

• In a support having a pore-size distribution, the largest pores will break first, then successively smaller and smaller ones. This occurs because the relative volume of the pore to support is highest for larger pores, and, thus, even though the stress exerted at the pore wall is the same or lower in a large pore, the stress in the support will be higher near the larger pores.

The model presented in this work is more of a descriptive model than a predictive one. Too many parameters need to be adjusted at the current time in order for it to be characterized as a fully predictive model without extensive experimental investigation. Furthermore, it is evident that the pore-size distribution and shape needs to be extremely well characterized in order for this model to be adapted to describe full-scale particle fragmentation. However, the model is useful for increasing our quantitative understanding of the physics of particle fragmentation, and to be able to predict what effects come out of changing parameters such as the polymer crystallinity (or anything else that changes its elastic or viscous properties).

In addition, in order for us to be able to use the approach suggested in this model, we would necessarily have a full 3-D model of particle morphology. In the case of an $MgCl_2$ support, this implies at least a statistical breakdown of the different particle fragment sizes, and the size of the bridges of support material holding them together. In the case of silica support, a much better description of the support morphology is needed, but with the same objectives in mind.

This model should also be characterized as a local model that describes fragmentation and morphology development in a small portion of the catalyst particle. For it to be integrated into a more complete single-particle model, the equations of mass and heat transport and the equations for particle growth should be included as well.

Acknowledgments

The authors thank the Norwegian Research Council (NFR) under the Polymer Science Program for financial support, and Borealis AS for supplying data on polymers.

Notation

A = specific surface area per volume, m^2/m^3
A_0 = specific surface area per mass, m^2/kg
a = primary elastic coefficient (= $2G + \lambda$), Pa
b = secondary elastic coefficient (= λ), Pa
E = Young's modulus of elasticity, Pa
G = Lamé's primary elastic coefficient, Pa
I = unit tensor
L = length of pore, m
p = pressure, Pa
R = reaction rate, variable
R_0 = peak reaction rate, kg/kg/h
R_m = reaction rate per mass, kg/kg/h
R_v = velocity reaction rate, m/s
R'_v = dimensionless velocity reaction rate
r = position variable (radius), m
r' = dimensionless radius
r_p = pore radius, m
r_i = inner radius of polymer shell, m

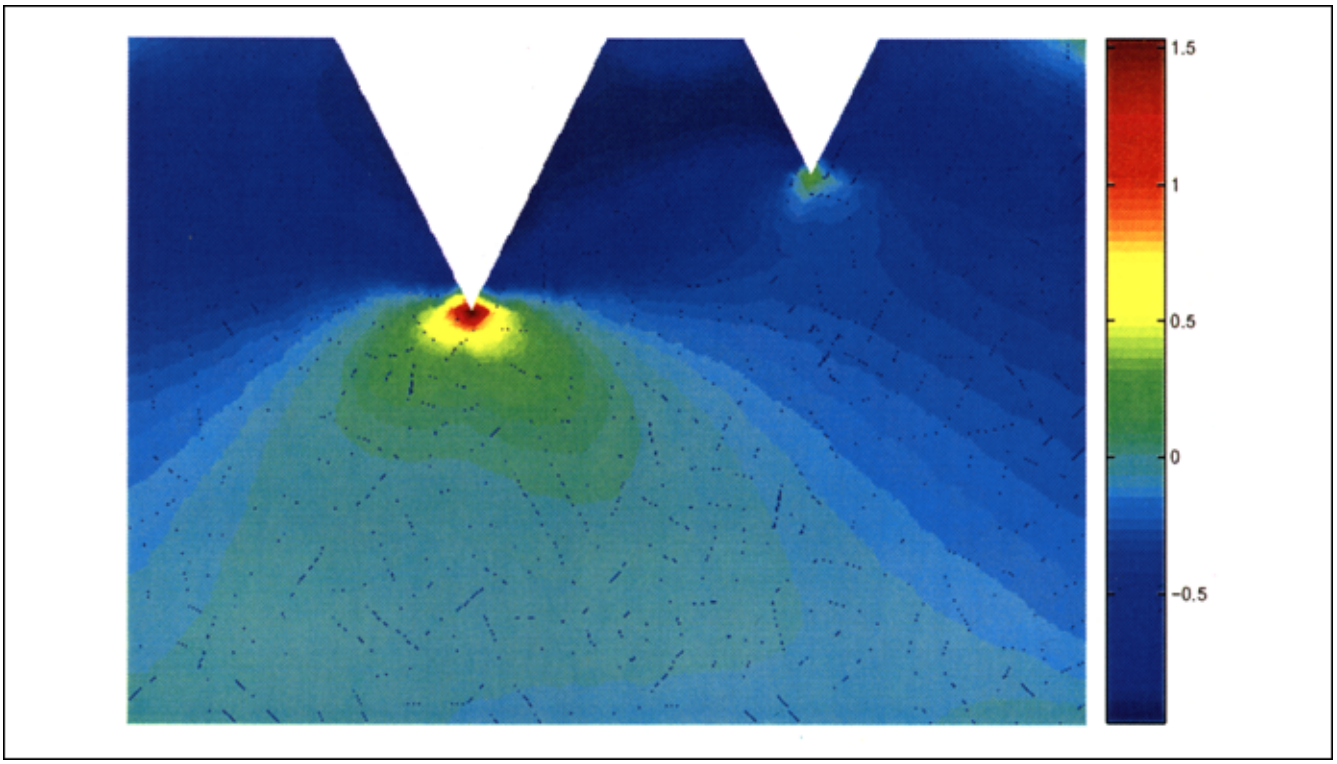

Figure 7. Stress (in horizontal direction) in a large and small pore with the same interfacial pressure applied.

The largest stress will be found at the inner point of the largest pore. The pore walls act as "crowbars" on the pore inner point. The numbers on the figure can be considered as relative values, and do not have a direct meaning.

r_s = outer radius of support shell, m
$\boldsymbol{T}$ = total stress tensor, Pa
t = time, s
t' = dimensionless time
t_{end} = polymerization time, s
t_{fill} = filling time of a pore if polymer were incompressible and inviscid, s
U = displacement function, m
w = width of new polymer shell, w

Greek letters

α = width of new polymer shell, w
β = primary viscous coefficient, Pa·s
ϵ = secondary viscous coefficient, Pa·s
ϵ_{ii} = strain in ith direction
ϵ_{ii}^{e} = elastic strain in ith direction
ϵ_{ii}^{v} = viscous strain in ith direction
ϵ_0 = initial porosity of catalyst particle
η = polymer viscosity, Pa·s
δ = Kronecker delta
κ = polymer bulk viscosity, Pa·s
λ = Lamé's secondary elastic coefficient, Pa
ν = Poisson's ratio
ρ = position variable, m
ρ = density, kg/m^3
σ = stress tensor, Pa
σ' = dimensionless stress
σ_{ii} = stress in ith direction, Pa
σ_{ii}^{e} = elastic stress in ith direction, Pa
σ_{ii}^{v} = viscous stress in ith direction, Pa
σ_i^{s} = stress in support in ith direction, Pa
σ_r^{w} = radial stress in polymer at support wall, Pa
$\bar{\sigma}_t^{s}$ = area average tangential stress in support, Pa
τ = relaxation time, s
τ_k = kinetic time constant, s

Literature Cited

Agarwal, U. S., and P. Lemstra, "Modeling Viscoelastic Resistance of Deposited Polymer During Olefin Polymerization," *Chem. Eng. Sci.,* **56**, 4007 (2001).

Agarwal, U. S., "Modelling Olefin Polymerization on Heterogeneous Catalyst: Polymer Resistance at the Microparticle Level," *Chem. Eng. Sci.,* **53**, 3941 (1998).

Bird, R. B., W. E. Stewart, and E. N. Lightfoot, *Transport Phenomena,* Wiley, New York (1960).

Boresi, A. P., and K. P. Chong, *Elasticity in Engineering Mechanics,* Elsevier, New York (1987).

Estenoz, D. A., and M. G. Chiovetta, "A Structural Model for the Catalytic Polymerization of Ethylene Using Chromium Catalysts. Part I: Description and Solution," *Poly. Eng. Sci.,* **36**, 2208 (1996).

Ferrero, M. A., and M. G. Chiovetta, "Catalyst Fragmentation During Propylene Polymerization: Part I. The Effects of Grain Size and Structure," *Poly. Eng. Sci.,* **27**, 1436 (1987a).

Ferrero, M. A., and M.G. Chiovetta, "Catalyst Fragmentation During Propylene Polymerization: Part II. Microparticle Diffusion and Reaction Effects," *Poly. Eng. Sci.,* **27**, 1448 (1987b).

Ferrero, M. A., and M. G. Chiovetta, "Catalyst Fragmentation During Propylene Polymerization: Part III. Bulk Polymerization Process Simulation," *Poly. Eng. Sci.,* **31**, 886 (1991a).

Ferrero, M. A., and M. G. Chiovetta, "Catalyst Fragmentation During Propylene Polymerization: Part IV. Comparison between Gas Phase and Bulk Polymerization Processes," *Poly. Eng. Sci.,* **31**, 904 (1991b).

Ferrero, M. A., A. Koffi, R. Sommer, and W. C. Conner, "Characterization of the Changes in the Initial Morphology for $MgCl_2$-Supported Ziegler-Natta Polymerization Catalysts," *J. Poly. Sci., Part A: Poly. Chem.,* **30**, 2131 (1992).

Ferrero, M. A., R. Sommer, P. Spanne, K. W. Jones, and W. C. Conner, "X-Ray Microtomography Studies of Nascent Polyolefin Particles Polymerized Over Magnesium Chloride-Supported Catalysts," *J. Poly. Sci., Part A: Poly. Chem.,* **31**, 2507 (1993).

Floyd, S., K. Y. Choi, T. W. Taylor, and W. H. Ray, "Polymerization of Olefins Through Heterogeneous Catalysis. III. Polymer Particle Modeling with an Analysis of Intraparticle Heat and Mass Transfer Effects," *J. Appl. Poly. Sci.,* **32**, 2935(1986).

Galli, P., "The Reactor Granule Technology: The Ultimate Expansion of Polypropylene Properties?," *J. Macromol. Sci., Chem.,* **A36**, 1561 (1999).

Galli, P., and J. Haylock, "Continuing Initiatro System Developments Provide a New Horizon for Polyolefin Quality and Properties," *Prog. Polym. Sci.*, **16**, 443 (1991).

Gao, P., and M. Mackley, "A General Model for the Diffusion and Swelling of Polymers and its Application to Ultra-High Molecular Mass Polyethylene," *Proc. R. Soc. London, A*, **444**, 267 (1994).

Jastrzebski, Z., *The Nature and Properties of Engineering Materials*, 3rd ed., Wiley, New York (1986).

Kittilsen, P., T. F. McKenna, H. Svendsen, H. Jakobsen, and S. Fredriksen, "The Interaction Between Mass Transfer Effects and Morphology in Heterogeneous Olefin Polymerization," *Chem. Eng. Sci.*, **56**, 4015 (2001).

Kittilsen, P., and T. F. McKenna, "A Study of the Kinetics, Mass Transfer, and Particle Morphology in the Production of High-Impact Polypropylene," *J. Appl. Poly. Sci.*, **82**, 1047 (2001).

Kosek, J., Z. Grof, A. Novak, F. Stepanek, and M. Marek, "Dynamics of Particle Growth and Overheating in Gas-Phase Polymerization Reactors," *Chem. Eng. Sci.,* **56**, 3951 (2001a).

Kosek, J., F. Stepanek, A. Novak, Z. Grof, and M. Marek, "Multi-Scale Modelling of Growing Polymer Particles in Heterogeneous Catalytic Reactors," ESCAPE-11, Copenhagen, Denmark (2001b).

Laurence, R. L., and M. G. Chiovetta, "Heat and Mass Transfer During Olefin Polymerization from the Gas Phase," *Polymer Reaction Engineering: Influence of Reaction Engineering on Polymer Properties,* K. H. Reichert and W. Geisler, eds., Hanser, Munich (1983).

McKenna, T. F., and J. B. P. Soares, "Single Particle Modelling for Olefin Polymerization on Supported Catalysts: A Review and Proposals for Future Developments," *Chem. Eng. Sci.,* **56**, 3931 (2001).

Pater, J. T. M., P. Roos, G. Weickert, K. R. Westerterp, F. Shimitzu, and G. Ko, *Integral Research Aspects of Gas Olefin Polymerization: Kinetics, Adsorption and Fluidization,* Dechema Monographs, Vol. 134, Wiley, New York, p. 103 (1998).

Pater, J. T. M., "Prepolymerization and Morphology," PhD Thesis, University of Twente, Enschede, The Netherlands (2001).

Simonazzi, T., G. Cecchin, and S. Mazzaullo, "An Outlook on Progress in Polypropylene-Based Polymer Technology," *Prog. Poly. Sci.,* **16**, 303(1991).

Van Krevlin, D. W., *Properties of Polymers*, 3rd ed., Elsevier, Lausanne, Switzerland, (1990).

Webb, S., E. Weist, M. Chiovetta, R. Laurence, and W. Conner, "Morphological Influences in the Gas Phase Polymerization of Ethylene by Silica Supported Chromium Oxide Catalysts," *Can. J. Chem. Eng.,* **69**, 665 (1991).

Weickert, G., G. B. Meier, T. M. Pater, and K. R. Westerterp, "The Particle as Microreactor: Catalytic Propylene Polymerizations with Supported Metallocenes and Ziegler-Natta Catalysts," *Chem. Eng. Sci.,* **54**, 3291 (1999).

White, F. M., *Viscous Fluid Flow,* McGraw-Hill, New York (1974).

Manuscript received June 19, 2002, and revision received Nov. 13, 2002.